Atomistic Simulation of Orientation of Methyl Groups and Methylene Bisectors, and Surface Segregation, in Freely Standing Thin Films of Atactic Poly(ethylene-*co*-propylene)

Sagar S. Rane, Wayne L. Mattice,* and Ali Dhinojwala

Department of Polymer Science, The University of Akron, Akron, Ohio 44325-3909

Received: October 6, 2003; In Final Form: June 29, 2004

Atomistically detailed models of free-standing thin films of random poly(ethylene-*co*-propylene) were produced using a method recently applied to atactic polystyrene (Clancy, et al. *J. Phys. Chem. B* **2001**, *105*, 11493). Monte Carlo simulations of the copolymer were carried out at ethylene fractions that cover the entire range of composition investigated in a recent experimental work (Opdahl, et al. *J. Phys. Chem. B* **2002**, *106*, 5212) based on sum-frequency generation (SFG) spectroscopy. We find that there is a minor enrichment of methyl groups on the surface, as compared to the bulk composition. Interestingly, the orientation distribution of methyl and methylene units is not unimodal. For methyl units, there is about 50% probability of orientation perpendicular to the surface. The other 50% are randomly oriented. For the methylene bisector, the simulation shows that the distribution has two broad peaks at opposite angles (at 180° apart) to the surface normal. More conclusive results may be obtained by using larger sample sizes and analysis of a larger number of snapshots, both of which increase the computation time significantly. The opposite angle pairs nearly cancel each other in the computation of an average order parameter and give us a misleading net result that the bisectors are randomly oriented. With increasing ethylene fraction, the orientation distribution of methyl and methylene units tends to become more uniform; however, this change is small. The strong average orientation of methyl groups and weak average orientation of methylene groups is in agreement with experiments. However, the simulation does not show the significant relative increase in the surface methyl groups contributing to the SFG signal as compared to the bulk concentration or an increase in average orientation of methylene units, with an increase in the ethylene fraction, as inferred from the experimental results. We find that the raw experimental data obtained with an increase in ethylene fraction can be explained by the changes in the number of methyl and methylene groups on the surface rather than the increase in surface excess of the methyl groups contributing to the SFG signal, trans cancellation, and increase in orientation of methylene bisectors as deduced from the experiments.

Introduction

The understanding of properties of polymer surfaces is crucial for the development of new technologies in areas such as adhesives, adsorption, wetting, and catalyst. One such property of interest is the segregation and structure of the side chains or side groups of the polymer chain and the backbone units at the surface or interface, in terms of their orientation and their concentration. A recent experimental technique, viz., IR−visible sum-frequency generation (SFG) spectroscopy has been widely applied to study the orientation pattern on the surface of several polymers and copolymers.[1−5] In general, it is reported that, for all systems investigated so far, side groups are found to orient outward and normal to the free surface. Simulation results[6,7] on selected homopolymers are in agreement with the experimental results by SFG. Recently,[5] SFG has also been used to study surfaces of random poly(ethylene-*co*-propylene) with a focus on understanding the effect of changing ethylene fraction on the surface structure. Since SFG signals are sensitive to both concentration and orientation, it is not straightforward to isolate the influence of these two terms independently. In this paper, we present an atomistically detailed model of the copolymer studied in ref 5 in freely standing thin film geometry and apply it to investigate the results drawn from the experimental work.

The simulation technique, based on coarse graining, allows us to control polymer tacticity, equilibrate relatively long polymer chain melts, and study the experimental system in detail by recovering the fully atomistic model through reverse mapping. The freely standing thin film is made from a model for the bulk polymer, by extending one direction of the periodic cell used for the simulation several times, followed by reequilibration of the model.[8] During the reequilibration the polymers cannot interact with their periodic images in the direction along which extension occurs. Due to the attractive van der Waals interactions between the beads, the chains collapse, resulting in the formation of a film, the thickness of which depends on the number of chains in the box and the length of the box in the two periodic directions. This method has been used previously for the construction of models of thin films of several polymers, such as polyethylene (PE),[9] polypropylene (PP),[10,11] polystyrene,[6] *cis*-1,4-polybutadiene,[8] polybenzoxazine,[10] random copolymers,[13] and sequentially ordered copolymers of ethylene and propylene.[10] The interface between the melt and vacuum has been studied using many different simulation techniques and models.[7,14−20] The first lattice simulation of this interface was performed by Madden[15] using a film adsorbed on a solid surface with one face exposed to the vacuum. In 1990, Mansfield and Theodorou[7] reported an atomistically detailed simulation of a thin film of glassy atactic polypropylene. An orthorhombic simulation cell was used, and a steep potential was applied at the cell faces normal to the longest direction in order to confine the chains and generate the thin film. Off-lattice Monte Carlo (MC) simulations on films of a bead-spring homopolymer

10.1021/jp037000g CCC: $27.50
Published on Web 08/24/2004

system were performed by Kumar et al.[20] In this work it was shown that a hypothetical plane called "the Gibbs dividing plane" separates the liquid- and gas-side regions around the interface. The chains on the liquid side exhibit meltlike characteristics near a hard wall, whereas the chains on the gas side possess a more collapsed configuration. Molecular dynamics simulations have also been employed to study the interface formed by films of alkane oligomers C_{10} and C_{20}.[19] The results of these fully atomistic simulations qualitatively agree with those from MC simulations on model systems of flexible chains.

Our coarse-grained model has the ability to capture the subtle effects arising from differences in stereochemical composition, as demonstrated by a recent work[21] which reproduces the known miscibility patterns[22−24] of mixtures of isotactic, syndiotactic, and atactic polypropylene melts. Thus, our coarse-grained model can successfully mimic the subtle interactions in multichain systems containing multiple species. For the copolymer under consideration in this work, similar subtle effects arising from small differences in the Lennard-Jones (L-J) parameters, ϵ and σ, of ethylene and propylene beads need to be incorporated. Our simulation method, as applied recently to polyethylene melts,[9,25] has been reviewed recently.[26,27]

Method and Simulation Details

For the simulation, coarse-grained chains are used which retain every second carbon atom in the main chain. Therefore each bead of the chain represents an ethylene or propylene monomer. These coarse-grained chains are placed on a high coordination lattice, the 2nnd lattice,[28,29] that contains $10i^2 + 2$ sites in shell i and an angle of 60° between any two axes. In the case of polypropylene bead, it is the α carbon atom that occupies a site on the 2nnd lattice. The step length on the lattice, 2.5 Å, is the distance between second nearest neighbor carbon atoms. Each lattice site can be occupied by one bead.

The coarse-grained models are simulated by a dynamic Monte Carlo algorithm[28] at 343 K, using a Hamiltonian that has two parts. One part is derived from the mapping of a rotational isomeric state model[30,31] for polyethylene,[32,33] polypropylene,[29] and ethylene−propylene copolymers[34] onto the coarse-grained chains. This part of the Hamiltonian enforces the proper distribution of mean square dimensions for each chain, and for its subchains, and also maintains the stereochemical sequence initially assigned to each chain. The second part of the Hamiltonian incorporates the intermolecular interactions. It uses a discrete version of a continuous Lennard-Jones potential energy function, given by methods introduced by Cho and Mattice.[35]

The first stage of the simulation was carried out on the coarse-grained 2nnd lattice, as done before for polypropylene[21,29] and polyethylene.[9] For every ethylene fraction under consideration, the appropriate bulk density at 343 K (70 °C) was calculated. The densities of polyethylene and atactic polypropylene (aPP) were taken as 0.825 and 0.832 g/cm^3, respectively.[36] Each chain consisted of 50 beads. In each chain, the sequence of ethylene and propylene beads was chosen at random, their total number being set by the overall ethylene fraction. Then, the number of chains used in the initial simulation of the melt was calculated by making sure that the right density is obtained in a box of 50 × 50 × 50 Å^3. Using this method, for pure PE, 31 chains were used, and for pure PP, 21 chains were used. After the melt is converted to a thin film, the system is free to choose its own density. For the propylene beads, the meso and racemo stereoisomers were assigned randomly to obtain an atactic polypropylene chain. The simulation was done for aPP, and three ethylene fractions in the chain, viz., 0.19, 0.42, and 0.75. Equilibration uses single bead moves[37] and pivot moves of 2−6 beads.[38] A Monte Carlo step (MCS) is the length of the simulation that attempts one move, on an average, for each bead and each type of move.

TABLE 1: Shell Energies (kJ/mol) Employed in the 2nnd Lattice Simulation

interaction	PE−PE	PP−PP	PE−PP
ϵ/k_B (K)	185	237.1	209.4
σ (Å)	4.4	5.118	4.759
first shell	11.078	20.593	14.810
second shell	0.196	1.995	0.872
third shell	−0.636	−1.145	−0.896

In the second stage of the simulation, the coarse-grained model was reverse-mapped to its fully atomistic model in continuous space. The atomic composition of a reverse-mapped chain is $C_{100+50f}H_{202+100f}$, where f denotes the mole fraction of propylene units. The atomistic model was then energy-minimized in steps, and the final equilibrated structure was obtained and used for our analysis.

Short-Range Energy. A rotational isomeric state model of a copolymer of ethylene and propylene was applied to include the short-range interaction of beads along the chain as described by Mattice and Suter.[31] The values of the energies of the short-range intramolecular interactions were assigned as $E_\sigma = 2.1$ kcal/mol, $E_\tau = 3.8$ kcal/mol, $E_\omega = 8.0$ kcal/mol, and $E_\eta = 0.29$ kcal/mol as obtained from the RIS model for polypropylene[39] and polyethylene.[32] In addition to this, the three types of pentane effect second-order interaction energies in propylene, viz., E_ω, $E_{\omega XX}$, and $E_{\omega X}$, were set equal to each other.

Long-Range Energy. The long-range interactions between ethylene and propylene beads were introduced on the 2nnd lattice by discretizing the continuous Lennard-Jones potential function as described by Cho and Mattice.[35] Previously tested values for the L-J potential of ethylene[9] and propylene,[40] which are suitable for simulation on the 2nnd lattice, were used. The L-J values for the ethylene−propylene interaction were estimated using the well-known Lorentz−Berthlot mixing rule. The various shell energies applied on the 2nnd lattice are shown in Table 1. Since the minimum in the L-J potential, at $2^{1/6}\sigma$, is near the boundary between the second and third shells for PE−PE (4.9 Å), and in the initial part of the third shell for PE−PP and PP−PP (5.34 and 5.74 Å, respectively), only the first three shells were used for computational efficiency, implying a cutoff distance of 7.5 Å in the long-range interaction. The energies of the fourth and higher shells are negative and much closer to zero than the energy in the third shell.

Thin Films. Models of the thin films were prepared from equilibrated models of the bulk, using a procedure described previously in detail[9] and applied to models of freely standing thin films of polyethylene[9] and polystyrene.[6] The procedure is summarized here in abbreviated form with the aid of Figure 1. Part a depicts a single parent chain in two dimensions. In the bottom panel of part b, each segment of this parent chain, at x_p and z_p, produces copies at $x_c = x_p \pm iL_x$ and $z_c = z_p \pm jL_z$, where i and j independently can be zero or any positive integer. The dashed lines in the bottom panel of part b denote the periodic boundaries defined by L_x and L_z. In actual practice, there is more than one parent chain, and the system is periodic in three dimensions. A single parent chain and two dimensions are employed in Figure 1 to minimize the clutter. Equilibration of the system in three dimensions, taking due account of the interpenetration of the parents and the copies, is a standard procedure for generation of models for dense amorphous

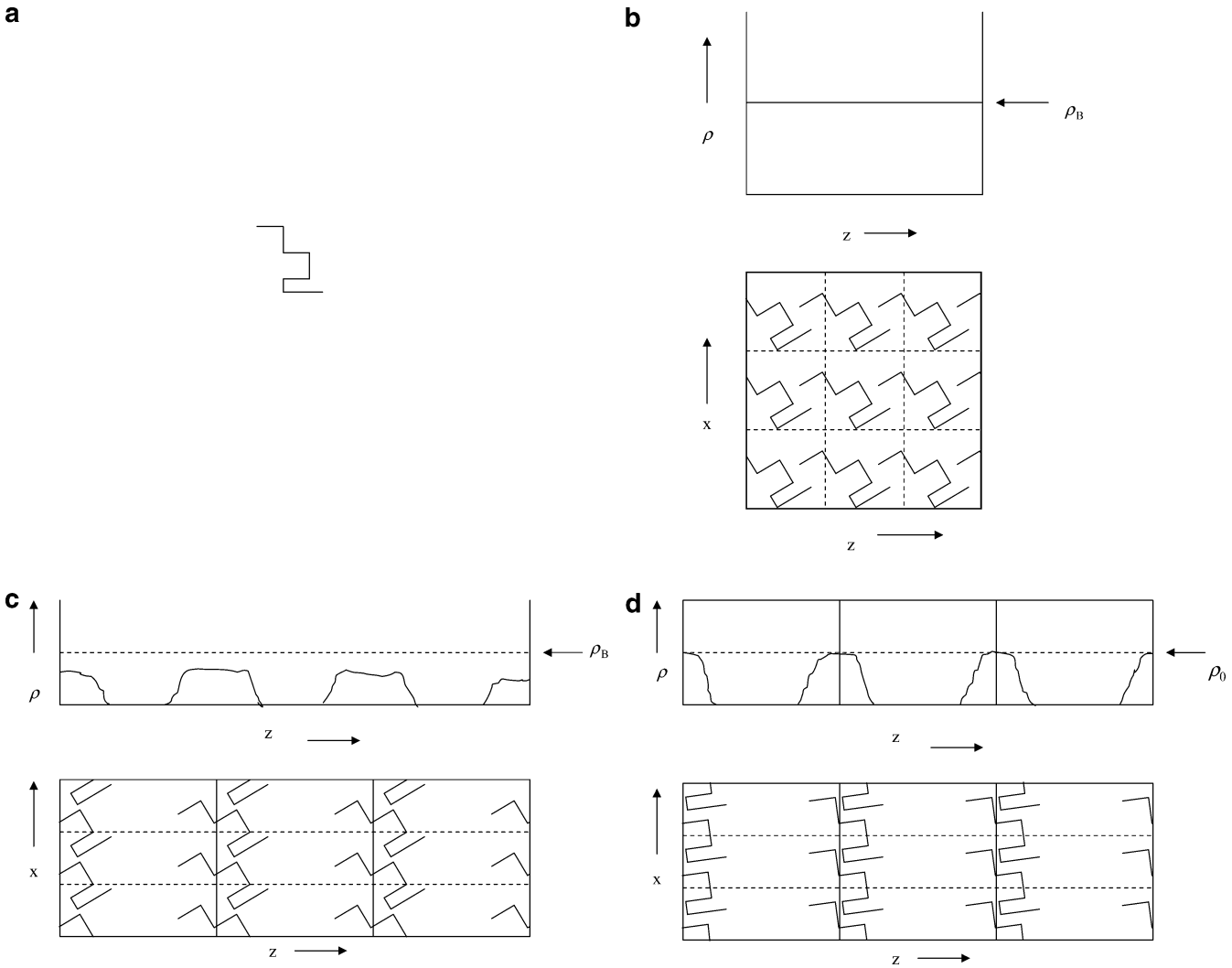

Figure 1. Different stages involved in producing models of freely standing thin films. Part a depicts a single parent chain in two dimensions. Part b shows the parent chains placed in a simulation box with periodic boundary conditions (shown by dashed lines) in the *x*- and *z*-directions. The images of parent chains are also shown. The top panel shows the density as a function of *z* for this situation. Part c depicts the situation obtained from part b by increasing the length of the simulation box in the *z*-direction by a factor of 4. The parent chains and its images still interact in the *x*-direction but not in the *z*-direction. Part d shows the structure obtained by equilibrating the chains in part c. The plateau density, ρ_0, of the final thin films is also shown in the top panel.

polymers.[41] The top panel of part b shows the density as a function of *z* for this situation. If the periodic boundaries are chosen appropriately, this density will be the bulk density for the melt, ρ_B.

The only change in proceeding from part b to part c is an increase by a factor of 4 in the size of L_z. The parent chain (and its images) have not changed their orientation or internal configuration. The density as a function of *z* is never as high as ρ_0, and there are substantial regions over which the density is zero. The parent and images still interact in the *x*-direction, but the value of L_z has been made too large to permit interaction in the *z*-direction. If there is no change in the configuration of the chains, the system is out of equilibrium.

Part d is obtained from part c by reequilibrating the chains, subject to the new periodic boundary conditions. Chains cannot feel their images along the *z*-axis, because L_z is too large. The attractive van der Waals interactions cause each set of chains to collapse with its images along the *x*-axis (and *y*-axis, in three dimensions) to form regions with bulk density. After equilibration, the density along the *z*-axis shows regions where $\rho = \rho_0$. On each side of one of these regions, the density falls from ρ_0 to zero in a manner described by a hyperbolic tangent function. The regions of nonzero density are separated by long stretches where no matter is present. In three dimensions, the system is an infinite set of thin films spaced by a new value of L_z, with the surfaces of the films equilibrated under exposure to a vacuum.

The two surfaces on either side of the high-density region are essentially independent of one another if the model is large enough so that a plateau region with bulk density is recovered in the middle of the film, and if the order parameters (which find anisotropy in the surface regions, where ρ is changing rapidly) become those of an isotropic system in the plateau region. When applied to atactic polystyrene, this approach gave excellent agreement with experimental results.[6]

In the present simulation of the ethylene−propylene copolymers, the film is first equilibrated on a high coordination lattice for 40 million MCS using the standard Metropolis criterion for acceptance of moves. The length of the simulation is chosen well-exceed the equilibration time, which is monitored in two ways: first by making sure that the mean square displacement of both kinds of beads in the chain is of the order of the thickness of the film and second the autocorrelation function of the end-to-end vector, $\langle r(t + t_0) \cdot r(t_0) \rangle$, goes to zero. Then the initial

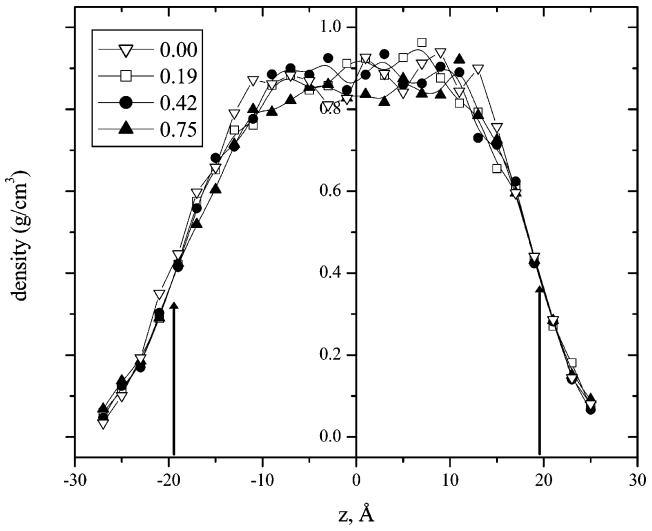

Figure 2. Density profile (g/cm^3) normal to the surface of the film for ethylene fractions of 0.00 (aPP), 0.19, 0.42, and 0.75. The vertical arrows show the location of the Gibbs dividing plane. The location of the Gibbs plane is almost identical for the four films with different ethylene fractions.

equilibrated structure is reverse-mapped to obtain full atomic coordinates depending on the stereochemistry of the chains. The reverse-mapped models are then energy-minimized by using the Discover force field and the stepwise procedure as described by Doruker and Mattice[37] with the Cerius^2 modeling software from Accelrys Inc. The energy minimization causes the atomistically detailed model to fall into a local conformational energy minimum in continuous space, that is close to the state in discrete configuration space produced by the previous Monte Carlo simulation with the coarse-grained model. The final structure is more strongly influenced by the methods and parameters employed in the extensive Monte Carlo simulation than by the force field adopted in the energy minimization.

Results and Discussion.

Density Profiles. In Figure 2 we show the density profile of the thin film along with the *z*-axis, which is normal to the surface. The position $z = 0$ is located in the middle of the thin film. The density profiles are averaged over eight independent reverse-mapped snapshots. The density in the middle of the film approaches roughly the bulk value ($\sim$0.83 g/cm^3) that is expected. At the surface, the density decays from the plateau value to zero over a distance of the order of 15 Å, which is typical for the simulations of the surfaces of polymeric hydrocarbons.[7−9] In the figure we also show the location of the Gibbs dividing plane,[20] as indicated by the vertical arrows. We find that the location of this plane is almost at the same position for the four films, and therefore we show only one location in the figure. In all figures, to ascertain we have statistically averaged results, we only show data points where the number of observables of study in that volume slab or bin is larger than 10.

Accuracy of the Model. The density profile at the interface can be fitted to the following hyperbolic tangent function[42]

$$\rho(z - z_{1/2}) = \frac{\rho_0}{2}\left[1 - \tanh\left(\frac{z - z_{1/2}}{\xi}\right)\right] \qquad (1)$$

where ρ_0 is the plateau density of the film, ξ is the correlation length, and $z_{1/2}$ is the value of z at which $\rho = \rho_0/2$. To provide additional support for the accuracy of our model and our claim that the final structure is more strongly influenced by our Monte Carlo simulation methods on the coarse-grained chains, rather than the force field employed in energy minimization, we perform the following calculations. Let $z_{cg;i}$ and $z_{at;i}$ denote the position of the Gibbs plane[20] for surface i in the coarse-grained replica and the atomistically detailed surface deduced from this replica. We will use the subscripts "cg" and "at" henceforth to denote quantities evaluated for the coarse-grained film and its atomistic replica, respectively. Then, possibly the best comparison between the images of the coarse-grained films and the atomistically detailed replica can be made through the root-mean-square difference in the values of z, i.e., $\langle(z_{cg;i} - z_{at;i})^2\rangle^{1/2}$. Similarly, the match between the coarse-grained and atomistically detailed replica can be judged by $\langle(\rho_{cg;i} - \rho_{at;i})^2\rangle^{1/2}$, which uses the plateau density, ρ_0, defined in eq 1. The width of the surface region in the two replicas can be compared through $\langle(\xi_{cg;i} - \xi_{at;i})^2\rangle^{1/2}$.

Let us denote by $z_{cg,i,j}$ the z coordinate of the coarse-grained bead j in the replica of film i used as a starting point for reverse mapping. Let $z_{at,i,j}$ denote the z coordinate of the carbon atom derived from this bead in the atomistically detailed model. Then the magnitude of the displacement along the z-axis as a consequence of reverse mapping is given by $\langle(z_{cg,i,j} - z_{at,i,j})^2\rangle^{1/2}$. In particular, the dimensionless ratio, $\langle(z_{cg,i,j} - z_{at,i,j})^2\rangle^{1/2}/\xi_i$ seems especially important, because it tells us whether the rearrangements are, or are not, important on the distance scale of the width of the surface region. In Table 2, we show these various quantities with different ethylene fractions in the chain. We also show the surface energy, and the overall fraction of CH_2-CH_2 bonds in the system in the trans state, p_t. From Table 2 we find that the coarse-grained film and its atomistically detailed replica match very well, and the rearrangement of atoms is not important on the scale of the width of the surface region as shown by the small numbers in the second to last column. We also find that our calculations give reasonable values for the surface energies that match with the values expected for simple amorphous polymeric hydrocarbons.[9,43] Previous simulations for thin films of copolymers with the repeating sequences (Et−Pr) and (Et−Et−Pr−Pr) gave surface energies of 30 $\pm$ 12 and 30 $\pm$ 8 erg/cm^2, respectively.[10] The typical uncertainties in the surface energies in our method are $\pm$10 erg/cm^2.[6] The plateau density, ρ_0, is also close to the bulk density expected by considering the composition of the chain, and the correlation length, ξ, is comparable to those obtained previously for other amorphous polymeric hydrocarbons.[44]

Later on we will also compare our results for the aPP surface with those obtained by Mansfield and Theodorou.[7]

TABLE 2: Various Quantities Which Depict the Accuracy of Our Model Calculations and the Dominance of Our Simulation Method on the Final Equilibrated Structure

ethylene fraction	ρ_0 (g/cm^3)	ξ (Å)	surface energy (erg/cm^2)	$\langle(z_{cg;i} - z_{at;i})^2\rangle^{1/2}$ (Å)	$\langle(\rho_{cg;i} - \rho_{at;i})^2\rangle^{1/2}$ (g/cm^3)	$\langle(\xi_{cg;i} - \xi_{at;i})^2\rangle^{1/2}$ (Å)	$\langle(z_{cg;i;j} - z_{at;i;j})^2\rangle^{1/2}/\xi_i$	p_t
0.00	0.87	5.78	30	0	0.01	0.63	0.17	N/A
0.19	0.86	5.42	31	0	0.035	0.19	0.18	0.68
0.417	0.85 5	5.11	30	0	0.01	0.01	0.21	0.64
0.75	0.86	5.54	27	0	0.04	0.36	0.23	0.60

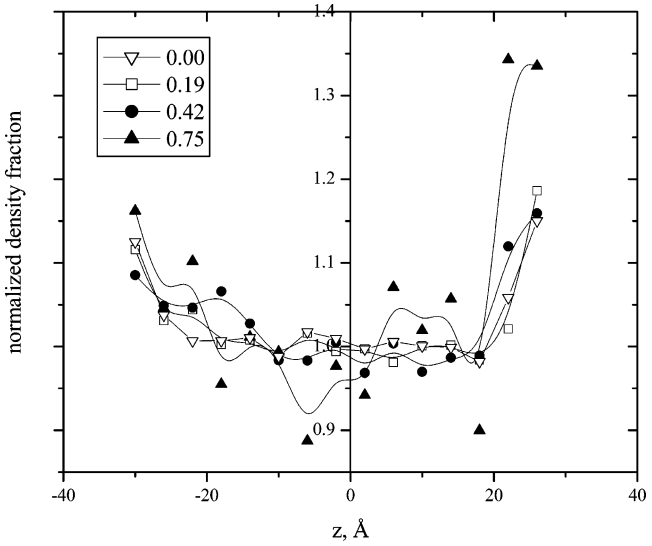

Figure 3. Normalized density profile for the methyl group as compared to the methylene group for the four different ethylene fractions. The normalization is done such that it will give the value of 1.0 if the relative density of the group in each bin is what is expected from the overall density of the repeat unit.

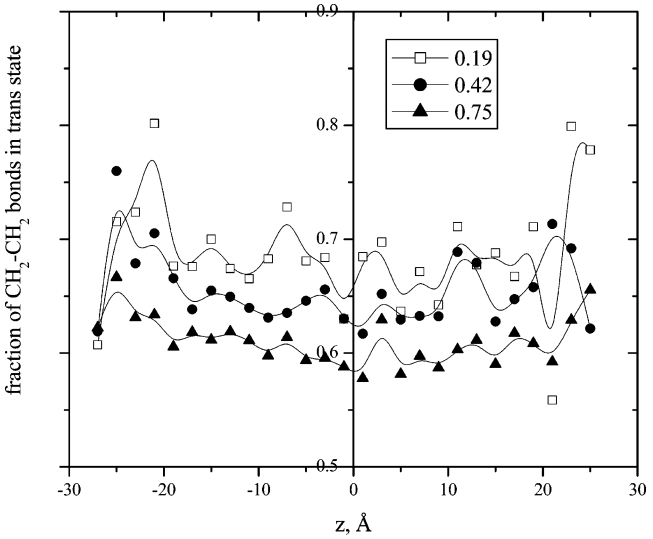

Figure 4. Fraction of CH_2-CH_2 bonds that are in the trans state, as a function of the distance from the center of the thin film, for the different ethylene fractions in the main chain. The results for aPP are not shown as there are not CH_2-CH_2 bonds in this polymer.

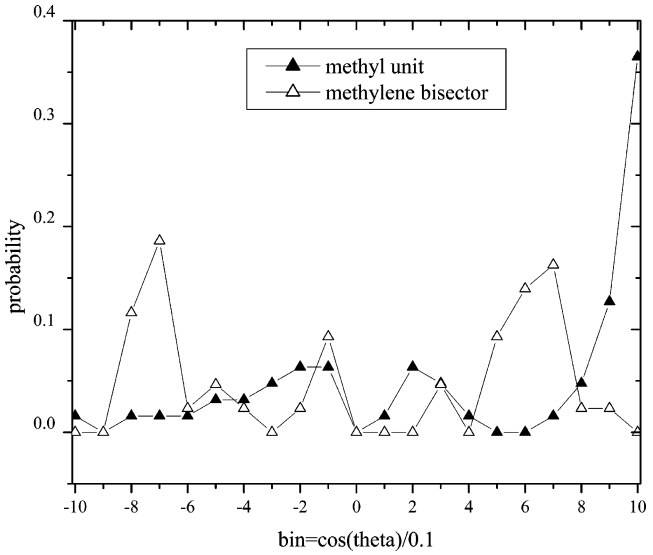

Figure 5. Orientation distribution of the methyl units and methylene bisectors for aPP in the volume slab at distances of 22−26 Å from the center of the film ($z = 0$). On the x-axis, the cos θ values are put into bins given by bin number = (cos θ)/0.1. The y-axis denotes the probability of having orientation given by that bin.

This comparison provides additional support for the accuracy of our model.

Normalized Density Profiles. In Figure 3, we show the normalized density profile for the methyl group for the four different ethylene fractions. The normalization is done such that it will give the value of 1.0 if the relative density of the group in each bin is what is expected from the overall density of the repeat unit. In the interior of the film, the normalized density is indistinguishable from 1.0. In the surface regions, the normalized density is slightly larger than 1.0. However, this enrichment is insignificant and is further discussed below.

To better understand the differences in the properties in the bulk and the surface, we calculate various quantities in the bulk; defined as the region between the two Gibbs planes as shown in Figure 2, and the surface (∼10 Å thick), which is the region outside the Gibbs planes. The results are shown in Table 3a. The data for the normalized density of CH_3 show that the surface may be slightly enriched in methyl groups and the enrichment may get stronger with increasing ethylene fraction. However, the enrichment is quite minor, ∼7% larger than the bulk composition at ethylene fraction of 0.42. In Table 3b, the same quantities are calculated by defining the surface by fitting eq 1 to the density profile. Here the surface is defined as the region beyond $z_{1/2} - \gamma/2$ on either side from the center of the film. The interfacial thickness (γ) is defined as the distance over which the density of the film decreases from 90 to 10% of its bulk value. Using this method, the surface is ∼16 Å thick.

Fraction of Trans Bonds. In Figure 4, we show the fractions of CH_2-CH_2 bonds that are in the trans state, as a function of the distance from the center of the film for the different ethylene fractions studied. The data for the surface and bulk regions are summarized in Table 3a,b. It is clear that the fraction of CH_2-CH_2 bonds in the trans state at the surface is practically identical to that in the bulk. As shown in Table 2, the overall fraction of CH_2-CH_2 bonds in the trans state are 0.68, 0.64, and 0.60 for ethylene fractions 0.19, 0.42, and 0.75, respectively. Thus, the overall fraction of CH_2-CH_2 bonds in the trans state appears to decrease with increasing ethylene fraction in the chains, although the decrease is minor.

Orientation of the Methyl Groups. The orientation of the methyl group is reported using the angle θ between the z-axis and the vector that points from the carbon atom that is bonded to the backbone to the carbon atom of the methyl group. In Figure 5 we show the orientation distribution of the methyl units of aPP at distances of 22−26 Å from the center of the film. This range falls in the surface region, as is evident through Figure 2. This distance slab was chosen for characterization because it falls in the surface region and the total number of observables in the slab is large enough to obtain a statistically averaged distribution. Within this distance slab, the orientations of the methyl units are characterized by putting the cos θ values into bins of width equal to 0.1. These bin values ranging from −10 to 10 along with the probability of having orientation in that bin are shown in Figure 5. The bin values are related to the cos θ values through bin number = 10 cos θ. Although there is a high probability for the methyl units to be oriented nearly along the z-axis (bin values = 8, 9, and 10), they collectively constitute only 50% of the probability. The remain-

TABLE 3: Comparison of Bulk and Surface

property	ethylene fraction	between planes (interior)	outside planes (surface)
(a) Comparison of Properties between the Two Gibbs Planes and Properties Outside of the Gibbs Planes (Approximately Top 10 Å of the Film)			
normalized density of CH_3	0.00	1.00	1.02
	0.19	0.99	1.03
	0.42	0.99	1.07
	0.75	0.98	1.19
fraction of CH_2-CH_2 bonds in trans state	0.00	N/A	N/A
	0.19	0.68	0.69
	0.42	0.64	0.69
	0.75	0.60	0.62
methyl group orientation	0.00	0.04, −0.03	0.32, −0.24
	0.19	0.04, −0.03	0.31, −0.22
	0.42	0.05, −0.02	0.30, −0.20
	0.75	0.06, −0.02	0.20, −0.20
methylene bisector orientation	0.00	0.00, −0.02	0.05, −0.07
	0.19	0.01, −0.02	0.01, −0.06
	0.42	0.00, −0.01	0.08, −0.05
	0.75	0.01, −0.01	0.05, −0.05
(b) Comparison of Properties in the Bulk and the Surface, When the Surface Is Defined by Fitting the Hyperbolic Tangent Function (Approximately Top 16 Å of the Film)			
normalized density of CH_3	0.00	1.00	1.01
	0.19	0.99	1.01
	0.42	0.99	1.03
	0.75	0.98	1.04
fraction of CH_2-CH_2 bonds in trans state	0.00	N/A	N/A
	0.19	0.68	0.69
	0.42	0.64	0.65
	0.75	0.60	0.61
methyl group orientation	0.00	0.00, 0.00	0.23, −0.18
	0.19	0.02, −0.02	0.20, −0.16
	0.42	0.02, 0.00	0.20, −0.15
	0.75	0.04, 0.01	0.17, −0.16
methylene bisector orientation	0.00	−0.01, −0.02	0.04, −0.04
	0.19	0.00, 0.00	0.02, −0.06
	0.42	0.00, −0.01	0.04, −0.04
	0.75	0.00, 0.00	0.04, −0.04

ing methyl units adopt orientations covering the entire range of the remaining θ values.

Similar results for the orientation distribution of methyl units were obtained for other ethylene fractions (results not shown). However, with increasing ethylene fraction the orientation distribution tends to become more uniform. To understand the methyl unit orientation as a function of the distance from the surface, we can determine $\langle \cos \theta \rangle$ from the orientation distribution, as shown for aPP in Figure 5. The location of the midpoint of the vector that points from the carbon atom that is bonded to the backbone to the carbon atom of the methyl group is used for assigning the orientation values to different bins in the *z*-direction. The order parameter, $\langle \cos \theta \rangle$, is 1.0 if this vector points in the positive *z*-direction, −1 if it points in the negative *z*-direction, and zero when there is no preferred orientation. The results for methyl group orientation with distance from the center of the film, at four different ethylene fractions, are shown in Figure 6. The summary in Table 3a,b reports separately the results at the two different surfaces ($z > 0$ and $z < 0$) in order to preserve the sign of the order parameter. We find that, as reported earlier,[6] the order parameter is not distinguishable from zero in that portion of the film where the local density is very close to the bulk value. Only in the surface region, where the density drops significantly from the bulk value we find the order parameter distinguishable from zero. At the outermost layers, the order parameter approaches values near ±0.5. Thus, at the two surfaces, the methyl groups are pointing outward and try to align normal to the surface, as has been observed previously in other simulations.[6,7,10] We also find that the orientation of methyl groups is not affected by the increasing ethylene fraction.

We find that due to the broad orientation distribution of methyl units, as shown in Figure 5 for aPP, the average value of cos θ gives extremely misleading information on the orientations adopted at the surface. E.g., for the methyl units in Figure 5, the value of $\langle \cos \theta \rangle$ is 0.45 (bin = 4−5); however; we note that there are practically no methyl units in that orientation.

Orientation of the Methylene Units. The orientation of the methylene units is reported through the orientation of its bisector, defined as the sum of the two C−H vectors that originate at the carbon atom and terminate at a hydrogen atom. In this case, θ is defined as the angle between the bisector and the *z*-axis. The orientation of methylene units reported here includes the methylene units in both the ethylene and propylene monomers. In Figure 5 we show the orientation distribution of the methylene units of aPP at distances of 22−26 Å from the center of the film. Within this distance slab, the orientations of the methylene units are characterized by putting the cos θ values into bins of width equal to 0.1. The bin values are related to the cos θ values through bin number = 10 cos θ.

The methylene bisector orientation distribution shows a trend much different from that of the methyl units. As shown in Figure 5, the methylene bisectors have higher probability for orientation at opposite θ values. These values are in the vicinity of θ = 45.57 and 134.42 (−45.57). However, there are other methylene bisectors with θ values that cover the entire range of possible orientations. Similar results were obtained for the orientation of methylene units at other ethylene fractions of 0.19, 0.42, and 0.75 (results not shown). However, with increasing ethylene fraction, the orientation distribution of methylene bisectors

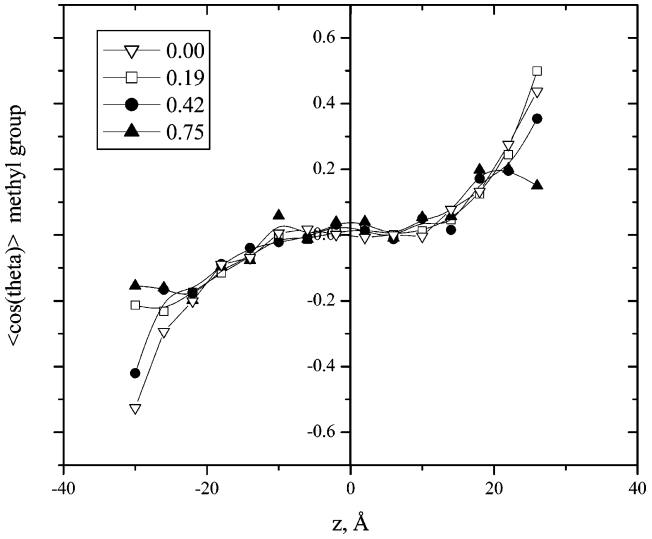

Figure 6. Order parameter of the methyl side group as a function of the distance from the middle of the film for four different ethylene fractions in the chains. The horizontal axis originates at the midpoint of the thin film.

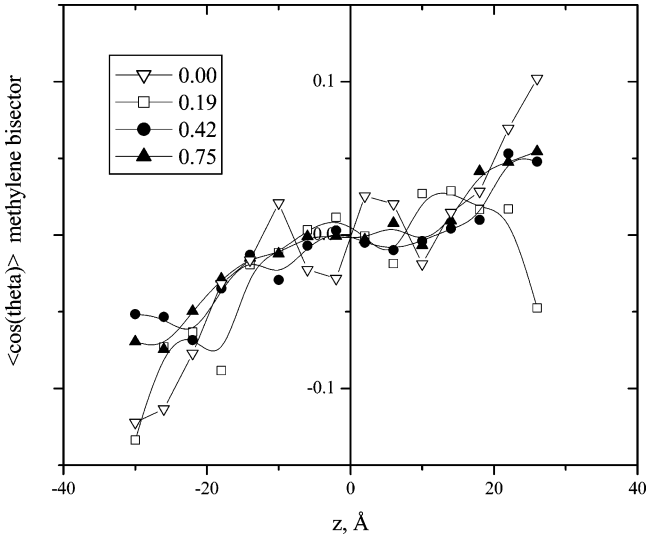

Figure 7. Order parameter of the bisector of the methylene groups as a function of the distance from the middle of the film for four different ethylene fractions in the chains.

appeared to become more uniform, therefore; the higher probability of orientations at ±45.57 should not be taken as absolute. Better statistics on the distribution obtained by using larger sample sizes and by analyzing a larger number of snapshots may give more conclusive results. To understand the methylene bisector orientation as a function of the distance from the surface, we can determine $\langle \cos \theta \rangle$ from the orientation distribution as shown for aPP in Figure 5. In Figure 7 we show the value of $\langle \cos \theta \rangle$ for the bisector for four ethylene fractions, and the data are summarized in Table 3a,b as before. We conclude, from the order parameter $\langle \cos \theta \rangle$, the methylene units are randomly oriented in the bulk. The average orientation at the surface can be best described as weak and unaffected by changing ethylene fractions. This is consistent with previous results for the average orientation of bisectors of methylene units in polystyrene.[6]

From Figure 5, we find that because there are pairs of bisectors with opposite θ values, around $\theta = \pm 45.57$, and there is a uniform distribution at other θ values, the average orientation, $\langle \cos \theta \rangle$, gives misleading information on their

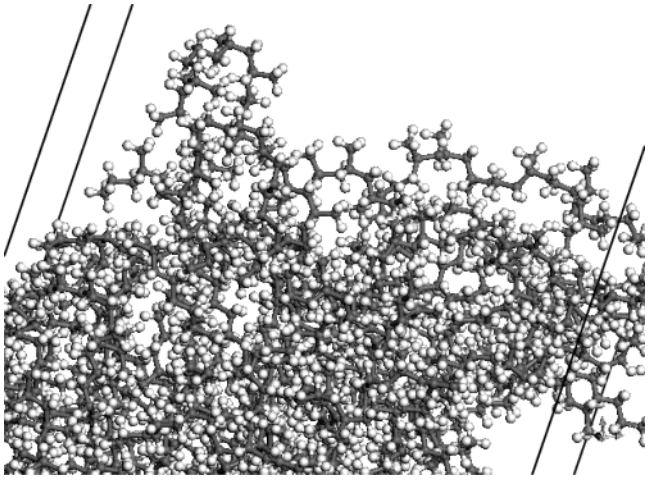

Figure 8. Snapshot of the surface of a freely standing thin film, with ethylene fraction 0.42, viewed from outside. The *z*-axis is along the vertical direction. The straight lines are the edges of the periodic cell used in the simulation.

preferred orientation. In Figure 5, which shows results for aPP, the methylene bisectors have $\langle \cos \theta \rangle \cong 0.09$. Again, as noted previously for methyl units, although for the bisectors $\langle \cos \theta \rangle \cong 0.09$, there are practically no bisectors (bin = 0−1) at this orientation.

Representative Snapshot. In Figure 8 we show a snapshot of the surface of the thin film, viewed from the side of the box, with the *z*-axis along the vertical direction. The straight lines in the figure are the edges of the periodic cell used in the simulation. As shown in Table 3a,b, the surface region has both methyl and methylene units and there is practically no segregation of these units. The methyl units are more strongly oriented along the *z*-axis than the methylene bisectors.

Comparison of aPP Data. Structure and properties of the atactic polypropylene thin film exposed to the vacuum has been previously studied by Mansfield and Theodorou.[7] We now compare the results of our model calculation with ref 7 and highlight the similarities and differences between the two calculations.

Temperature and Degree of Polymerization. The simulation in ref 7 was done for a glassy aPP surface at a temperature of −40 °C. Our simulation temperature (70 °C), however, is well above the glass transition temperature for aPP. This large temperature difference will make the comparison difficult; nevertheless, we try to make a qualitative comparison. The degree of polymerization employed in ref 7 is 76, which is slightly larger than our degree of polymerization of 50.

Density Profile. In ref 7, the interfacial thickness is defined as the distance over which the mass density falls from its bulk value to almost zero. Using this definition, they find that the interfacial thickness is less than 10 Å. From Figure 2, we find that this distance is about 15 Å. The larger thickness may be assigned to the higher temperature in our simulation.

In ref 7, the total density profile rises sharply as one goes from the surface into the bulk and a shallow minimum is obtained near the surface. In our simulation, as shown in Figure 2, the density profile is hyperbolic and no shallow minimum exists.

Mansfield and Theodorou[7] find that the outermost (low-density) surface region is richer in methyl groups than the bulk. We also get similar results. However, this enrichment is minor, as shown in Table 3a.

Order Parameter. Using a different order parameter, $S = [3\langle \cos^2 \theta \rangle - 1]/2$, Mansfield and Theodorou[7] studied the

orientation of skeletal C−C, pendant C−H, and pendant C−CH_3 bonds at different distances from the surface. They found that both the C−H and C−CH_3 bonds try to align perpendicular to the surface, near the surface. We only have our C−CH_3 average bond orientations to compare with the above results. From Figure 6, we find that our results agree with the results of ref 7.

Mansfield and Theodorou[7] also studied the chain center of mass distribution, and the variation in the overall shape and orientation of entire chains with the distance from the surface. We have, however, not characterized these properties.

Comparison with Experimental Data. Using the information of the number of methyl and methylene units and their order parameter with distance from the center of the film, we can compare the simulation results to those determined from recent SFG measurements.[5] Before we proceed with the comparisons, we briefly summarize the main principles of the SFG technique. SFG is a nonlinear optical spectroscopic technique, where two laser light beams of frequencies ω_1 and ω_2 are overlapped on a medium to produce a beam at the sum of the two source frequencies, $\omega_3 = \omega_1 + \omega_2$. The SFG (assuming the electric dipole approximation) is forbidden in media with inversion symmetry. However, at the interface between two centrosymmetric media, inversion symmetry is broken and generation of the SFG signal is allowed. The ω_2 in SFG experiments is a tunable infrared laser, and the SFG signals are enhanced near the infrared resonances of the molecules. The position of the resonance peak determines the identity of the molecules at the interface (in this case methyl and methylene groups). As a broad simplification, the SFG intensity is related to the product of the number of groups at the interface and the average orientation. The definition of the interface for polymers is not straightforward, and it is not necessary that the number of groups contributing to the SFG intensity reside in the immediate vicinity of the interface. The contribution to the SFG signal will be zero when the average $\langle \cos \theta \rangle \sim 0.0$ in the bulk, which is the 10−20 Å region near the surface. In experiments, a ratio of SFG intensities in two different combinations of incoming and outgoing polarization of light is used to determine the average orientation. After knowing the average orientation and some form of an absolute calibration, one can determine the number of groups at the interface. To relate this number to surface concentration prior knowledge of the orientation distribution is required. In particular, the situation is more complicated when non-unimodal distribution exists, such as the one observed in the current system. Most often the orientations and surface compositions are compared relative to another; for example, in recent work,[5] copolymer results are compared with the results from aPP.

Orientation of Methyl and Methylene Units. The distribution of the orientation determined from the simulation is not unimodal, and, therefore, the comparison with experiments requires some assumptions. Experimentally, it was determined that the methyl groups are oriented normal to the surface and this orientation does not change with the increase in the ethylene fraction. Since the SFG orientation calculations are insensitive to the methyl groups that are oriented randomly, we only compare the 50% methyl units that fall in bins 8, 9, and 10 (Figure 5). If we use these units, then the simulation results agree with the experiments. Also, approximately 50% of the methyl units remain vertically oriented with an increase in the ethylene fraction. However, we would like to reiterate that this does not imply that all the methyl units at the surface are oriented normal to the surface. There are around 50% methyl units that are distributed randomly at the other angles. On average, the $\langle \cos \theta \rangle$ is 0.45 (for aPP), rather than 1.0 if they were all oriented normal to the surface.

TABLE 4: Analysis of the Surface

	for given ethylene fraction			
	0.00	0.19	0.42	0.75
(a) Analysis of the Surface Defined by the Gaslike Side of the Gibbs Dividing Plane				
$n_{CH_3,\,surface}$	77	66	51	29
$n_{CH_2,\,surface}$	69	86	108	165
R1	231	226	224	266
R2	207	207	198	211
R3	0.89	1.30	2.11	5.69
(b) Analysis of the Surface Defined by Fitting the Hyperbolic Tangent Function to the Interfacial Density Profile				
$n_{CH_3,\,surface}$	295	246	196	95
$n_{CH_2,\,surface}$	281	343	446	644
R1	885	842	863	871
R2	843	826	818	824
R3	0.95	1.39	2.27	6.78

For the methylene units, it is not obvious which units should be considered. For the methylene bisector, the distribution has two broad peaks at opposite angles (at 180° apart) to the surface normal. If we consider the average orientation, $\langle \cos \theta \rangle$, then we obtain a value that is very close to zero. The weak average orientation of methylene units is also observed in the experiments. However, the order parameter of methylene groups does not change with the increase in ethylene fraction as suggested from the experiments.

Number Density of Methyl and Methylene Units at the Surface. In Table 4a,b, we determine various ratios obtained from the simulation results that will be helpful in comparison with the experimental work.[5] In each table, a different surface region is identified. In Table 4a, the gaslike side of the Gibbs dividing plane is defined as the surface ∼10 Å thick. In Table 4b, the surface is defined as the region beyond $z_{1/2} - \gamma/2$ on either side from the center of the film. This method defines the surface as ∼16 Å thick. These different choices in defining the surface allow us to compare the results and evaluate the effect of different surface thickness.

In each table, we show the number of methyl groups ($n_{CH3,surface}$) and methylene groups (n_{CH2},surface) on the surface, and the three ratios $R1 = n_{CH3,surface}/[CH_3]_{bulk}$, $R2 = n_{CH2,surface}/[CH_2]_{bulk}$, $R3 = n_{CH2,surface}/n_{CH3,surface}$. These ratios have been characterized in the experimental work[5] as a function of changing ethylene fraction, using the PP homopolymer as the reference system. As mentioned before, SFG experiments can only report the number density and orientation of species that contribute to the signal; hence, in ref 5, $n_{CH3,surface}$ and $n_{CH2,surface}$ refer to those molecules. However, we find that the distribution function (or the ordered fraction) of methyl and methylene units does not change with the ethylene content. Hence, the above three ratios based on absolute surface composition in fact measure the change in the methyl and methylene units contributing to the SFG signal relative to the bulk concentration, as done in ref 5, and can be readily compared with that data. In our case, the three ratios are calculated without any reference system.

We find that R1 is almost a constant over the ethylene fraction range 0.00 to 0.75. This contrasts with the experimental work where R1 increases by almost 50% as the ethylene fraction increases from 0 to 0.42. R2 is also almost a constant. In contrast, in the experimental work, R2 decreases by almost 30% as the ethylene fraction increases from 0 to 0.42. We find that R3 *increases* substantially with increasing ethylene content. In

ref 5, however, R3 remains unchanged with the ethylene content. These ratios help us in understanding the variation in the surface composition as the ethylene content in the chains is changed. The ratios show that in absolute numbers, the surface gets richer in methylene units and depleted in methyl units as the ethylene content in the chains is increased.

As evident from Table 3a, the surface composition is slightly richer in methyl units as compared to the bulk composition. However, this enrichment is quite minor [~7% at ethylene fraction of 0.42 (Table 3a), the highest ethylene fraction studied by experiments]. If we consider the other definition of the surface based on fitting the hyperbolic tangent function (Table 3b), the surface enrichment is even smaller (~3% at ethylene fraction of 0.42). The highest enrichment of ~19% was observed with the surface defined using the Gibbs plane (Table 3a), at an ethylene fraction of 0.75. This information on the absolute surface composition is not available from the SFG experiments in ref 5. However, comparing the three ratios R1 through R3 have shown that the simulation results do not agree with the experimental findings. According to our simulations, the ordered fraction is almost unchanging and the surface gets slightly enriched in methyl groups relative to the bulk composition, with increasing ethylene fraction (Figure 3). This does not agree with the conclusions drawn in ref 5 that the ordered fraction of the methyl groups itself increases with increasing ethylene fraction.

Our results compare favorably with those from several studies[45−47] based on applying XPS and other techniques to characterize the composition at the air− polymer interface of random copolymers and block copolymers with different block lengths. It agrees with the general hypothesis that there is no surface segregation in random copolymers. At least one study[48] has suggested that significant surface enrichment of one component may occur for block copolymers only when the block length exceeds a certain critical length. Finally, XPS studies on ethylene−propylene random copolymers also show that the surface composition scales as the bulk composition.[49,50]

Fraction of Ethylene Bonds in Trans State. As shown in Figure 4, the simulation results find that the fraction of CH_2-CH_2 bonds that are in the trans state at the surface *decreases* with increasing ethylene content. The experimental work suggested that an *increasing* fraction of methylene units adopt a trans conformation on the surface as the ethylene content increases.

It is clear that although there is qualitative agreement of the orientation of methyl and methylene units, the surface excess results do not match with the prediction from experiments. One potential reason may be the difficulty in separating the contribution of orientation and the number density of methyl and methylene groups at the surface from SFG spectroscopy. This is particularly difficult, knowing that the orientation distribution is not uniform and unimodal.

To compare the simulation results directly to SFG results without trying to decouple the orientation and number density, we have determined the changes in the SFG vibrational mode strengths expected for the methyl and methylene units and the ratio of the methylene/methyl mode strengths as a function of the ethylene fraction. Since the orientations of methyl and methylene groups remain more or less the same with an increase in ethylene fraction, the changes in the vibrational mode strengths should be proportional to the density of the molecules at the surface. From Table 4a, we expect that the decrease in the symmetric methyl mode strength in going from aPP to the ethylene fraction of 0.42 is ~33%. This is in reasonably good agreement with the decrease of ~13% found in ref 5. As

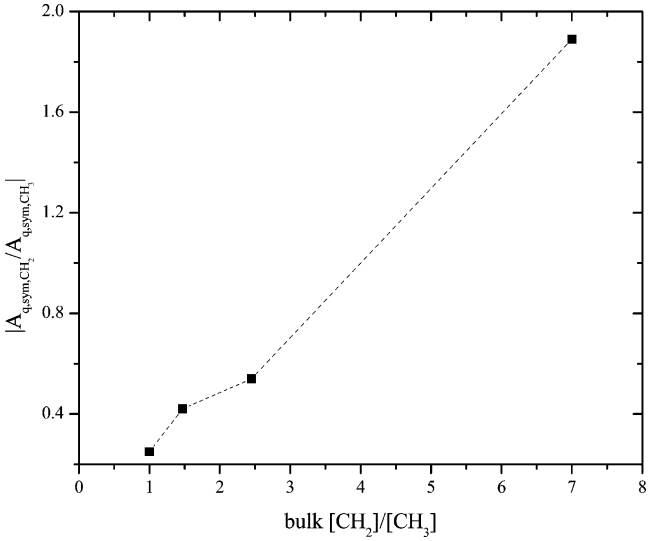

Figure 9. Ratio of CH_2(s)/CH_3(s) ssp vibrational mode strengths (A_q) as a function of the bulk $[CH_2]/[CH_3]$ ratio.

mentioned before, we also find that roughly 50% of the methyl units remain oriented perpendicular to the surface as the ethylene fraction is increased. Therefore, including these groups into the mode strength calculation will not affect the conclusion reached above. For the SFG intensity from methylene units too, good agreement is observed between the simulation and experiments. Also, the symmetric methylene mode strength, which is predicted to increase by ~56% in going from aPP to the ethylene fraction of 0.42, is in reasonably good agreement with the experimentally observed increase of ~77%. Thus, the simulation agrees with the experiments on the raw data.

We have also calculated the ratio of CH_2(s)/CH_3(s) ssp vibrational mode strengths (A_q) as follows:[51]

$$\left|\frac{A_{q,sym(ssp),CH2}}{A_{q,sym(ssp),CH3}}\right| = \left|\frac{n_{CH2}\beta^{CH2}{}_{ccc}[(r^{CH2}+2)\langle\cos\theta^{CH2}\rangle + (r^{CH2}-2)\langle\cos^3\theta^{CH2}\rangle]}{2n_{CH3}\beta^{CH3}{}_{ccc}[(r^{CH3}+1)\langle\cos\theta^{CH3}\rangle - (1-r^{CH3})\langle\cos^3\theta^{CH3}\rangle]}\right|$$

where r^{CH2} or (r^{CH3}) is the ratio of $\beta^{CH2}{}_{aac}/\beta^{CH2}{}_{ccc}$ (or $\beta^{CH3}{}_{aac}/\beta^{CH3}{}_{ccc}$). We have taken $r^{CH2} = 1.64$,[52] $r^{CH3} = 2.24$,[53] and $\beta^{CH3}{}_{ccc}/\beta^{CH2}{}_{ccc} = -0.5$,[54] to construct the ratio of $A_{q,sym(ssp),CH2}/A_{q,sym(ssp),CH3}$ as a function of the bulk $[CH_2]/[CH_3]$ ratio, shown in Figure 9. The corresponding figure in the experimental work[5] is their Figure 5. As shown in Figure 9, we find that the ratio of the mode strengths increases with increasing ethylene concentration in the bulk; this is in agreement with the experimental work. However, the changes in the SFG raw data can be related to the changes in methyl and methylene groups at the surface.

Conclusions

Atomistic simulations of random atactic poly(ethylene-*co*-propylene) in freely standing thin films were conducted by reverse mapping an equilibrated intermediate structure from the coarse-grained model. The results show that the distribution of the orientation of the methyl and methylene units at the surface is not unimodal. For the methyl units, there is a high probability for orientation along the surface normal; however, they make up only about 50% of the methyl units. The remaining units have orientations that cover the entire range of remaining θ values. For the methylene units, there is high probability for

orientation at opposite θ values in the vicinity of $\theta = \pm 46$ (most valid for aPP), although all other θ values are also significantly populated. With increasing ethylene fraction, the orientation distribution of methylene bisectors appeared to become more uniform, therefore; the higher probability of orientations at ± 46 should not be taken as absolute. Better results for the distribution could be obtained by using larger samples sizes in the simulation and by averaging orientations over more snapshots. The contribution of these opposite θ values in the methylene bisector cancel each other out and give an $\langle \cos \theta \rangle$ that is slightly larger than zero. However, the methylene units can be considered as ordered, in pairs of opposite orientations. The average orientation, $\langle \cos \theta \rangle$, of neither species is affected by changing the ethylene content. The simulation results indicate that the surface is slightly enriched with the methyl units as compared to the bulk composition. However, this enrichment is minor for all the ethylene fractions studied in this work. The fraction of CH_2-CH_2 bonds in the trans state were not found to increase in the surface region or with increasing ethylene content in the chains. The simulation results agree with the relative changes in the ratio of SFG intensity[5] of methylene/methyl peaks with increasing ethylene fraction. However, they do not agree with the relative changes in the number of methyl and methylene units contributing to the SFG intensity with increasing ethylene fraction as inferred in the experiments. In addition, the increase in the relative contribution to the methylene signal is due to increase in the n_{CH2}/n_{CH3} ratio at the surface, rather than the surface excess of methyl groups contributing to the signal, trans cancellation, and increase in the order parameter of methylene groups as suggested in the experimental work.

Acknowledgment. This work was support by National Science Foundation Grants DMR 0098321 and DMR 9984996 (A.D.).

References and Notes

(1) Gautam, K. S.; Schwab, A. D.; Dhinojwala, A.; Zhang, D.; Dougal, S. M.; Yeganeh, M. S. *Phys. Rev. Lett.* **2000**, *85*, 3854.
(2) Briggmann, K. A.; Stephenson, J. C.; Wallace, W. E.; Richter, L. J. *J. Phys. Chem. B* **2001**, *105*, 2785.
(3) Zhang, D.; Shen, Y. R.; Somorjai, G. A. *Chem. Phys. Lett.* **1997**, *281*, 394.
(4) Oh-e, M.; Lvovsky, A. I.; Wei, X.; Shen, Y. R. *J. Chem. Phys.* **2000**, *113*, 8827.
(5) Opdahl, A.; Phillips, R. A.; Somorjai, G. A. *J. Phys. Chem. B* **2002**, *106*, 5212.
(6) Clancy, T. C.; Jang, J. H.; Dhinojwala, A.; Mattice, W. L. *J. Phys. Chem B* **2001**, *105*, 11493.
(7) Mansfield, K. F.; Theodorou, D. N. *Macromolecules* **1990**, *23*, 4430.
(8) Misra, S.; Fleming, P. D.; Mattice, W. L. *J. Comput.-Aided Mater. Des.* **1995**, *2*, 101.
(9) Doruker, P.; Mattice, W. L. *Macromolecules* **1998**, *31*, 1418.
(10) Clancy, T. C.; Mattice, W. L. *Comput. Theor. Polym. Sci.* **1999**, *9*, 261.
(11) Xu, G. Q.; Mattice, W. L. *J. Chem. Phys.* **2003**, *118*, 5241.
(12) Kim, W. K.; Mattice, W. L. *Langmuir* **1998**, *14*, 6588.
(13) Natarajan, U.; Misra, S.; Mattice, W. L. *Comput. Theor. Polym. Sci.* **1998**, *8*, 323.
(14) Poser, C. I.; Sanchez, I. C. *J. Colloid Interface Sci.* **1979**, *69*, 539.
(15) Madden, W. G. *J. Chem. Phys.* **1987**, *87*, 1405.
(16) Kumar, S. K.; Vacatello, M.; Yoon, D. Y. *J. Chem. Phys.* **1988**, *89*, 5206.
(17) Theodorou, D. N. *Macromolecules* **1989**, *22*, 4589.
(18) Rowlinson, J. S.; Widom, B. *Molecular Theory of Capillarity*; Oxford University Press: New York, 1989.
(19) Harris, J. G. *J. Phys. Chem.* **1992**, *96*, 5077.
(20) Kumar, S. K.; Russell, T. P.; Hariharan, A. *Chem. Eng. Sci.* **1994**, *49*, 2899.
(21) Clancy, T. C.; Pütz, M.; Weinhold, J. D.; Curro, J. G.; Mattice, W. L. *Macromolecules* **2000**, *33*, 9452.
(22) Lohse, D. *Polym. Eng. Sci.* **1986**, *26*, 1500.
(23) Thomann, R.; Kressler, J.; Setz, S.; Wang, C.; Mülhaupt, R. *Polymer* **1996**, *37*, 2627.
(24) Thomann, R.; Kressler, J.; Rudolf, B.; Mülhaupt, R. *Polymer* **1996**, *37*, 2635.
(25) He, D.; Reneker, D. H.; Mattice, W. L. *Comput. Theor. Polym. Sci.* **1997**, *7*, 19.
(26) Doruker, P.; Mattice, W. L. *Macromol. Theory Simul.* **1999**, *8*, 463.
(27) Baschnagel, J.; Binder, K.; Doruker, P.; Gusev, A. A.; Hahn, O.; Kremer, K.; Mattice, W. L.; Müller-Plathe, F.; Murat, M.; Paul, W.; Santos, S.; Suter, U. W.; Tries, V. *Adv. Polym. Sci.* **2000**, *152*, 41.
(28) Rapold, R. F.; Mattice, W. L. *J. Chem. Soc., Faraday Trans.* **1995**, *91*, 2435.
(29) Haliloglu, T.; Mattice, W. L. *J. Chem. Phys.* **1998**, *108*, 6989.
(30) Flory, P. J. *Statistical Mechanics of Chain Molecules*; Wiley: New York, 1969.
(31) Mattice, W. L.; Suter, U. W. *Conformational Theory of Large Molecules. The Rotational Isomeric State Model in Macromolecular Systems*; Wiley: New York, 1994.
(32) Abe, A.; Jernigan, R. L.; Flory, P. J. *J. Am. Chem. Soc.* **1966**, *88*, 631.
(33) Rapold, R. F.; Mattice, W. L. *Macromolecules* **1996**, *29*, 2457.
(34) Mark, J. E. *J. Chem. Phys.* **1972**, *57*, 2541.
(35) Cho, J.; Mattice, W. L. *Macromolecules* **1997**, *30*, 637.
(36) Orwall, R. A. In *Physical Properties of Polymers Handbook*; Mark, J. E., Ed.; American Institute of Physics: Woodbury, NY, 1996; p 81.
(37) Doruker, P.; Mattice, W. L. *Macromolecules* **1997**, *30*, 5520.
(38) Clancy, T. C.; Mattice, W. L. *J. Chem. Phys.* **2000**, *112*, 10049.
(39) Suter, U. W.; Pucci, S.; Pino, P. *J. Am. Chem. Soc.* **1975**, *97*, 1018.
(40) Clancy, T. C.; Mattice, W. L. *J. Chem. Phys.* **2001**, *115*, 8221.
(41) Theodorou, D. N.; Suter, U. W. *Macromolecules* **1985**, *18*, 1467.
(42) Helfand, E. *J. Chem. Phys.* **1975**, *63*, 2192.
(43) Brandup, J.; Immergut, E. H. *Polymer Handbook*, 3rd ed.; Wiley: New York, 1989.
(44) Doruker, P.; Mattice, W. L. *J. Phys. Chem. B* **1999**, *103*, 178.
(45) Kumler, P. L.; Matteson, H. L. *Langmuir* **1991**, *7*, 2479.
(46) Chen, X.; Lee, H. F.; Gardella, J. A., Jr. *Macromolecules* **1993**, *26*, 4601.
(47) Zhuang, H.; Gardella, J. A., Jr. *Macromolecules* **1997**, *30*, 3632.
(48) Li, L.; Chan, C.-M.; Liu, S.; An, L.; Ng, K.-M.; Weng, L.-T.; Ho, K.-C. *Macromolecules* **2000**, *33*, 8002.
(49) Galuska, A. A.; Halverson, D. E. *Surf. Interface Anal.* **1998**, *26*, 425.
(50) Opdahl, A.; Phillips, R. A.; Somorjai, G. A. *Macromolecules* **2002**, *35*, 4387.
(51) Hirose, C. In *Advances in Multiphoton Processes and Spectroscopy*, Vol. 9; Lin, S. H., Villaeys, A. A., Fujimura. Y., Eds.; World Scientific: Singapore, 1995; p 145.
(52) Wei, X.; Hong, S. C.; Zhuang, X. W.; Goto, T.; Shen, Y. R. *Phys. Rev. E* **2000**, *62*, 5160.
(53) Zhuang, X.; Miranda, P. B.; Kim, D.; Shen, Y. R. *Phys. Rev. B* **1999**, *59*, 12632.
(54) Hirose, C. Private communication.